

The Geomagnetic Tail: Topology, Reconnection  
and Interaction with the Moon

C. P. Sonett, D. S. Colburn, R. G. Currie\*, and J. D. Mihalov

Space Sciences Division, Ames Research Center, NASA

Moffett Field, California 94035

FACILITY FORM 602

N 68-26328	(ACCESSION NUMBER)	(THRU)
52	(PAGES)	1
NASA-TMX#-60238	(NASA CR OR TMX OR AD NUMBER)	(CODE)
		30
		(CATEGORY)

GPO PRICE \$ \_\_\_\_\_

CFSTI PRICE(S) \$ \_\_\_\_\_

Hard copy (HC) 3.00

Microfiche (MF) .65



ff 653 July 65

\*National Academy of Sciences Postdoctoral Resident Research Associate

Presented at the Summer Institute, Physics of the Magnetosphere, Boston College,  
Chestnut Hill, Massachusetts, June 26, 1967

## ABSTRACT

A preliminary assessment of the geometry of the geomagnetic tail is made using data from the Ames magnetometer on the Explorer 33 satellite. The general shape corresponds to the earlier findings of Ness and co-workers. The tail is found regular to distances greater than  $82 R_e$ . The field values vary for  $K_p \leq 2+$  from a low of about 4 gamma to a high value of 40 gamma. Generally the values are in the neighborhood of 10 to 20 gamma. A distinct skewing of the field lines away from the solar-antisolar direction is observed, such that an added component of magnetic field in the direction of planetary motion is present on both sides of the null plane. The skewing appears to be greatest near the null plane. Increase in field magnitude with increasing  $K_p$  is observed. The radial gradient can be shown to fit a power or exponential law with near equal validity. A correlation analysis of field magnitude with radial distance,  $a_p$ , and transverse position coordinates also is discussed. Little cross gradient is observed in the tail field. Strong evidence for reconnection of field lines is found, and statistics are presented for a dual effect regarding the residual Z field across the null plane. Lastly the interaction of the tail field with the moon is discussed in terms of the mechanism of Sonett and Colburn.

## INTRODUCTION

This paper reports preliminary findings from the Ames Research Center magnetometer experiment on the Explorer 33 satellite regarding the extended magnetic tail of the earth, evidence for reconnection of field

lines at the neutral plane, field magnitude gradients in the tail structure and an early comparison of magnetic activity observed on earth and in the tail. The Explorer 33 satellite was launched on July 1, 1966; the orbit has the highest apogee so far achieved by an earth satellite. The initial apogee was  $4.37 \times 10^5$  km ( $68.55 R_e$ ) and perigee  $5.10 \times 10^4$  km ( $8.00 R_e$ ). Variations in the orbit parameters due mainly to lunar perturbations do not allow a statement of invariant orbital parameters. Ecliptic longitude of the major axis of the first orbit was 118 deg measured clockwise looking towards the south ecliptic pole, with 0 deg longitude along the earth-sun line; the corresponding ecliptic latitude was  $3.2^\circ$  S. Special properties of the orbit of value for the present study are the extreme distance from the earth, the long period, and the initial firing into the rearward direction away from the sun. Fig. 1 shows the first eleven orbits extending over five months. The approximate mean positions of the forward edges of the bow wave and magnetopause are shown. Coverage is especially favorable for spatially extended examination of the magnetic tail past the orbit of the moon.

During August and September alone nearly three weeks of relevant data are available. These are examined for the general extended topology of the tail, for details of the null plane crossings and for storm related modifications.

Since the discovery of the tail structure by Ness and co-workers, the general configuration has been mapped out (Ness, 1965; Fairfield and Ness, 1967), certain storm related phenomena have been discussed (Behannon and Ness, 1966) and the null sheet has been examined in detail (Spicer and Ness, 1967) and correlated with both low energy (Bame et al.,

1966; Bame et al., 1967) and high energy (Montgomery et al., 1965; Anderson, 1965; Anderson and Ness, 1966; Murayama, 1966) particle data. More recently it is reported that a wake extension of the tail is found to distances approaching  $10^3 R_e$  (Wolfe et al., 1967). This latter finding suggests tail breakup at lesser distances, the data having strong time-variant properties. The evidence from the Vela satellites indicates that an asymmetry exists in the plasma temperature, with the higher values found on the dawn side of the tail. General increases in the intensity of the tail field are described by Behannon and Ness (1966) during times of enhanced  $K_p$ . In the present paper the discussion is limited to the tail proper; the extended bow shock of the earth observed at lunar distance is reported in a subsequent publication, as are details of the far transition region.

For the present work the preferred coordinate system is solar magnetospheric. Separation between earth centered control of the tail and solar wind control is discussed later. However the radial coordinate,  $X_{sm}$  is identical in the solar magnetospheric and solar ecliptic systems and the definition of transit through the neutral sheet uses this variable.

#### INSTRUMENTATION

The Ames magnetometer is a triaxial flux gate, constructed from designs developed jointly by NASA/Ames Research Center and the Honeywell Radiation Center. The instrument has certain novel features used for the first time and so a brief description of the system is given. There are two primary assemblies consisting of the boom mounted package and the electronics mounted in the interior of the spacecraft. The former consists of the

three sensor elements,  $S_1$ ,  $S_2$ ,  $S_3$ , and a thermal motor for rotation of the  $S_2$  and  $S_3$  sensors through  $90^\circ$  once approximately every twenty-four hours. The rotation is such as to interchange the axes of the two sensors with respect to the spacecraft allowing inflight determination of the sensor offsets. The  $S_3$  sensor is oriented in the spacecraft spin axis direction on one day while the  $S_2$  sensor is oriented in the anti-spin axis direction the next day. The thermal motor is dual to compensate for changes in temperature of the housing due to different solar aspect. Also included is a thermistor for temperature monitoring of the assembly, and a sensor position detector for verification of the direction of the two sensors. The third sensor is oriented radially and is fixed in spacecraft coordinates. In summary the three sensors, each having the response of a free space dipole are mounted mutually orthogonally with one along the spin axis, and the other two orthogonal in the spin plane.

The magnetometer block diagram is shown in Fig. 2. The design is of the null type with feedback providing the null and the output signal. Calibration signals are injected into the feedback loop for verification of the scale factor of the instrument.

Signals from those sensors mounted in the spin plane of the spacecraft are intrinsically spin modulated, whereas the spin axis sensor signal contains Fourier components generated exclusively by the natural hydromagnetic radiation field. The spin modulation problem is especially severe in the present case since the telemetry bandwidth is insufficient for ground station demodulation which can be shown to be imperfect at best. We therefore include a pair of quadrature-synchronous phase-demodulators for rectification of these signals.

The reference direction is obtained from a sun pulse. The three outputs are then identical in format corresponding to the type of signals obtained from a nonspinning spacecraft. For the basic theory of spin modulation of hydro-magnetic signals and the criteria for spectral purity, the reader is referred to the literature (Sonett, 1966; Fredricks, Greenstadt, and Sonett, 1967).

The complete system consisting of magnetometer, spin demodulator, and alias filter and storage buffer system is shown in Fig. 3. The inclusion of the buffer storage is required to conserve bandwidth while observing the stringent alias contamination constraint required for the experiment. The three ranges used are  $\pm 20$ ,  $\pm 60$ , and  $\pm 200$  gamma. These are sampled sequentially while the axes are measured instantaneously with respect to all effective time constants. In this paper all data except 24 one-hour averages near the earth are taken with the 20 gamma range. Bypass data, which is not spin-demodulated, allows checking demodulator operation in space.

For calibration purposes the rotation of the sensor elements together with the imposition of a calibration current raster allows both the scale factor linearity and the offsets to be determined. Calibration signals are used during the general flipping cycle once per day.

The pre-alias filter used was a compromise between linear phase response and adequate protection against folding the higher frequency spectral components into the passband of the system which, for each range, has a Nyquist limit of 0.08 cps. At this frequency the alias contribution from a white noise or flat power spectrum background is 1%. Thus the response of the system droops appreciably at the higher frequencies but this effect is easily removed in spectral analysis by recoloring the

spectra. For most of the data in the present paper this problem is irrelevant. Data giving neutral sheet structure is filtered as described, however.

For some of the discussion, the question of sensor offset becomes relevant since residuals appear in the null sheet crossing. We therefore consider these effects now. A tabulation of sensor offset history through the first thirty weeks of operation discloses a drift of 1.0 gamma in sensor  $S_3$  upon which is superimposed a random variation of standard deviation 0.15 gamma. Sensor  $S_2$  has a random variation of approximately the same value for the same time period except that during a spacecraft turn-off due to battery problems near the end of calendar year 1966, an irreversible change of 0.85 gamma took place. By this time the spacecraft was spending most of its time in interplanetary space, so tail data was not available. The regular variations have been removed from the data discussed here. An additional check upon the instrument can be obtained from study of the switching spectrum associated with small variations in the leakage rate of the field effect transistors used in the buffer storage system. From these data it is possible to assert that leakage effects are less than 0.2 gamma, the equivalent of 1/2 digital window. In this preliminary examination the statistics of the switching tone errors are not sufficiently well known to provide the description for addition of these errors to those of the random variations in the probe offsets. The worst case assumption that the former is a steady state error superimposed upon the random variations of the probe offsets yields an overall error of less than one digital window (0.4 gamma). Effects associated with the spin demodulation system are generically connected with angular offsets. These are known from laboratory calibration to be of order 2-3

degrees or 0.05 radians, and therefore are unimportant in the assessment given here.

#### ORBIT AND COORDINATE SYSTEM

The primary coordinate system used in the analysis is solar-magnetospheric where  $\vec{X}_{sm}$  is defined as the unit vector along the radial line from the earth to the sun with positive sense towards the sun.  $\vec{Y}_{sm}$  and  $\vec{Z}_{sm}$  form the remaining two unit vectors of the mutually orthogonal set with  $\vec{Z}_{sm}$  in the plane containing  $\vec{X}_{sm}$  and a centered earth's geomagnetic dipole axis, and positive  $\vec{Y}_{sm}$  in the sense opposed to the planetary motion. Thus  $\vec{Z}_{sm} \times \vec{X}_{sm} = \vec{Y}_{sm}$  so that  $\vec{Y}_{sm}$  lies in the magnetic equatorial plane. (In the subsequent discussion the subscripts are dropped for simplicity.)

Therefore the magnetospheric system displays two periodic dependences, the daily wobble of the earth's magnetic dipole axis and the yearly wobble of the earth's spin axis, both with respect to the ecliptic.

The direction of  $\vec{X}$  is invariant to the solar magnetospheric and solar ecliptic coordinate systems. Therefore X-components of magnetic field or spacecraft position vectors are identical in the two coordinate systems. However, resolution of the Y- and Z-components of vectors will vary in the two systems, and a planar coordinate rotation is required. Consideration of such rotations is necessary in the null sheet study presented later.

The annual motion of the earth rotates the daily mean magnetic dipole equator of the earth through a range of  $\pm 23 \frac{1}{2}$  degrees. During the nearly six months of these observations, the rotation was from the minimum value to nearly the maximum as the tip of the earth's axis varied

from the summer to nearly the winter value. Superimposed upon this was the daily wobble of  $\pm 11.7$  degrees. Thus in orbital plots (Fig. 11) a diurnal effect is seen. Also the apparent trend in the coverage of the tail in magnetospheric coordinates is due to the annual variation which for the later orbits of the series used here takes the spacecraft to progressively more negative values of Z. Thus a sweep over a large range of both Y and Z is effected.

The present work is restricted in the sense that the relation of ecliptic to magnetospheric coordinates is not complete. Our evaluation of the relative control of either coordinate system is then based upon crossing of the null plane. Since this is determined partly by the effects of the solar wind, the comparison is not complete. Our basic intent is concerned with the null plane itself and gradients in the tail rather than the control problem which is treated elsewhere.

#### DEFINITION OF THE FIELD AVERAGE

A vector average can be expressed in at least two distinct manners. Sometimes the average over magnetic field samples is defined by

$$\overline{B}_1 = \frac{1}{j} \left[ \left( \sum_{i=1}^j B_{xi} \right)^2 + \left( \sum_{i=1}^j B_{yi} \right)^2 + \left( \sum_{i=1}^j B_{zi} \right)^2 \right]^{1/2} \quad (1)$$

An exact definition of the average direction angle of the kth component of the field,  $\overline{\delta}_k$ , is given by

$$\cos \overline{\delta}_k = \frac{\frac{1}{j} \sum_{i=1}^j B_{ki}}{\overline{B}_{MAG}} \quad (2)$$

where

$$\overline{B}_{MAG} = \frac{1}{j} \sum_{i=1}^j (B_{\pi i}^2 + B_{y i}^2 + B_{z i}^2)^{1/2} \quad (3)$$

is a more accurate definition of the average field magnitude. For purposes of composing a projection of the field into a plane for graphical representation it is required to use both (1) and (3) because a clear distinction exists between the two methods when the field is not time stationary. The most extreme case is a unit vector whose directions are uniformly distributed over a  $4\pi$  solid angle; equation (3) yields a unit magnitude while (1) yields a zero magnitude with an unbounded error. Sample analyses for five minute averages show that for moderately disturbed data swaths in interplanetary space the competing methods can yield percentage errors of 30%; for corresponding averages in the sheath 30% errors are common. Fig. 4 gives average field magnitude errors in two swaths of tail data using the competing methods and Fig. 5 shows the average difference between the magnitudes averaged over varying time intervals. Except when the satellite frequently cuts through the null sheet average percentage errors for tail data are generally less than 2%. The error vanishes for a time stationary field but the difference is significant even for very low frequencies provided that the spectral components are contained within the bandwidth of the averaging frequency. Use of Eq. (1) always depresses the magnitude values.

In the following sequence of discussions either or both Eqs. (1) and (3) are used. The averaging times are always of one hour or longer duration, except for the null sheet study.

## GENERAL FORM OF THE TAIL FIELD

Only a few magnetic field values for which at least one component in the spacecraft frame of reference exceeds 20 gamma are used in the analyses of this paper. Consequently every third vector is used, the others representing the 60 and 200 gamma ranges. Thus the field data is bounded to values  $>7 R_e$ . Fig. 6 gives projections of the component-magnitude composite averages of the magnetic field south of the null plane taken over orbits 1, 4, 5, 6, 7 and 8 representing over 12 weeks of data in the second half of 1966. The averages are over three hour intervals and give a representation of most of the tail field.

The general tendency of the field direction to lie toward or away from the solar direction agrees with previous results (Ness et al., 1967). In Fig. 7 we show the fields north of the null plane. Again the general configuration is tail-like. The primary new features in these data show the ordered extension of the tail to distances as great as the distance of the projection of satellite apogee into the X - Y or solar-magnetospheric plane, i.e.  $\sim 80 R_e$ . Thus the tail fields extend to a distance which suggests immersion of the moon during the full moon phase. The breadth of the fields in the X - Y plane implies that tail occultation of the moon extends over some 30 degrees of the lunar orbit. This suggestion results from the  $40 R_e$  lateral extension of the projected tail field at  $80 R_e$  radial distance.

The daily and annual oscillation of the orbit in magnetospheric coordinates indicates that the data shown are representative of the tail cross section and radial extension.

Examination of Fig. 7 shows that the field direction tends away from the anti-solar direction on the dusk side. It is not likely that this result is an unexplained offset in one or more of the magnetometer sensors since such a bias would affect the larger near-earth values less. In the orbits of Fig. 7 the geometry favors closer approach to the null sheet on the dusk side. One possibility for the skew therefore is that it grows with diminishing distance from the null plane. The skewing is discussed further in the next section.

The largest features show that the ordered field extends beyond  $80 R_e$  in the anti-solar direction and that the projection of the lateral extension of the field at these distances is of order  $40 R_e$ . A similar extension of the distant tail field is evident in the direction normal to the plane, i.e., Z. As seen especially in Figure 6, the fields in the tail are generally well ordered and regular on the scale of time used for the averaging.

#### SKEWING OF THE FIELD AWAY FROM THE ANTI-SOLAR DIRECTION

We consider further here the apparent skewing of the field shown especially in Fig. 7. Our earlier statement that the data appears biased to skewed values when in the neighborhood of the null plane is examined further.

On orbit 1 the spacecraft locus swings wide of the tail at the early part of the ascending leg. For  $|Y| < 12 R_e$  the fields are anti-solar and not less than  $25 \gamma$ . Beyond this distance there appears a general tendency for the field to rotate away from the X axis. For nearly all

these data the satellite is within  $5 R_e$  of the X-Y plane. At  $\sim 30 R_e$  on the flank the transition region is entered. Until this time the field is characterized by increasing angular spread from the X axis reaching a maximum of over 45 degrees just prior to the penetration.

On orbit 3 during the ascending leg the spacecraft was always within  $10 R_e$  of the X-Y plane. For the week during the ascending part of the orbit the field always displayed a direction away from -X. The form is characterized by increasing angle as the field magnitude increases nearer the earth and the spacecraft is nearer the null plane. Angles as large as 45 degrees are encountered at a radial distance of order  $20 R_e$ . Near apogee the deviation in angle decreases to  $\sim 5$  degrees. However the orbit 4 data distinctly show that upon crossing of the null plane the angle changes sign with respect to the -X direction. Thus the skewness is characterized by an angular change of  $\sim 10$  degrees.

A strong distinction is made in orbit 5 where all measurements used here are taken when  $Z > 10 R_e$ . A distinct relation appears in this case favoring skewing nearer the null plane.

Orbit 6 further demonstrates the condition of skewing for a case where greater values of -Z are encountered. Here again the neighborhood of the null is favored but for the measurements closer to earth ( $|Z| < 20 R_e$ ) and the null plane, the tendency to skew is strong as in the case of orbit 3.

Dessler and Juday (1965) have discussed the effects of planetary rotation upon the form of the geomagnetic tail and have concluded that the spin leads to twisting of the tail field. The sense of the twist is

such that in the northern half of the tail, a net contribution to the field in the direction of planetary motion is added on the null side of the lobe, and a contribution in the opposite direction is added on the top. The reverse is the case for the southern half of the tail. Our data disclose that the sense of the perturbation magnetic field which would account for the skewing is in the direction of planetary motion on both sides of the null plane and therefore cannot be accounted for by the rotation of the earth. It is possible to account for the observed skew by the addition of a current loop passing through the two lobes of the tail on either side of the null plane. The current flows earthwards in the lower or southern lobe and away from the earth in the upper lobe. We cannot state what the closure path would be and therefore the model lacks certain necessary details. On the other hand the equivalent current system must be specified. The decrease of field skewing away from the null plane indicates that the model suggested would require a decrease in the current density away from the null plane.

Skewing of tail fields could also be evidence for expansion of the size of the tail with increasing geocentric distance. On the dawn side, such skewing would simulate an added field component in the direction of planetary motion in the southern lobe, and in the opposite direction in the northern lobe. This configuration does not agree with observations either.

A specific cause of the observed skewing is not available. The observations could be explained if field twisting discussed by Dessler and Juday (1965) were dominant at the northern edge of the null sheet, and an effect due to tail divergence was dominant at the southern edge.

## RECONNECTION AND MERGING OF FIELD LINES

A sensitive test for reconnection of field lines is found from examination of the residual Z component of field often associated with crossings of the null sheet. The criterion used here for a crossing is a reversal in the algebraic sign of  $B_x$ . This definition has the advantage of independence from the ecliptic-magnetospheric coordinate systems. (An alternative definition would use minima in  $|\vec{B}|$  as a sign of the crossing.) Our criterion is that used by Speiser and Ness (1967). Our major conclusions are not altered if the alternate definition is used.

Since many of the crossings display strong time variations, i.e., reversal several times before the null neighborhood is left behind by the satellite, we strengthen the definition used here by the following requirements;  $B_x$  must change sign for at least two serial vector measurements, i.e. 12 seconds, and the reversal of  $B_x$  must equal or exceed 0.5 gamma for one of the two measurements. The rule allows a fluctuating null plane to be tabulated more than once, and generally the question of multiple crossings cannot be identified. Our query is independent of the number of adjoining crossings however.

The quantity investigated here is the algebraic sign of the Z component at the null crossing. Fig. 8 shows a swath of 127 samples of null crossings from the first orbit. Until  $35 R_e$  there is only one example of a negative residual in  $B_z$ . Beyond this point in radial distance there occur 20 additional negative values. Thus the ratio  $B_z(+)/B_z(-)$  is 5.8; 17% of the Z components are negative. Additional evidence for both positive

and negative crossing excesses is found in the swath from August 16 to 26 again covering most of orbit 4; during this time the ratio is 6.7. The third example we show in Fig. 9 discloses a ratio of  $B_z(+)/B_z(-) = 2$  for data from September 6 to 10 (i.e. about 33% of the crossings show negative excess). In all the data there is a strong tendency for the negative values to be found at the greater distance from the earth (such activity characteristically starts at  $\sim 35 R_e$  on orbit 1).

The occurrence of both positive and negative excess in the Z component can only mean that loops of field are witnessed crossing the null region. Either the radial field is severed and closed loops are formed, or kinks form closed loops in the field lines. The negative cases could be evidence for loops where the loop being observed is the outward part of a pair of loops formed in the severing. This is shown diagrammatically in Fig. 10. The enhanced statistical occurrence of positive values suggests that two processes are seen. The first is the severing or kinking of field and the second, suggested also by the radial gradient of tail field magnitude discussed later, is the continual presence of field loops pulled out from the magnetosphere. The latter do not suggest severance, but display only the natural polarity associated with the magnetospheric field. On this basis there appears a partitioning of loops where the bulk of the loops are a part of the drawn out magnetospheric field, while the remainder are connected with the severance of the radial tubes of flux and the formation of an equal fraction of positive and negative loop segments. Whether this hypothesis is correct depends upon considerably more data than available to us. On the other hand it is difficult to construct a model other than the one

proposed in order to explain the negative polarities frequently seen. The idea of field severance is a part of most current theories by which hot plasma is carried into the magnetosphere. We believe that these observations lend support to the possibility of rapid reconnection of field across null surfaces as proposed by Piddington (1960), Axford et al. (1965) and Coppi et al. (1966).

Our findings can be examined with respect to the open and closed magnetospheric models (Johnson, 1960). Insufficient data are available at the present time for a complete assessment, but a cursory examination strongly favors the magnetosphere which is open for a long distance. (The question of connection to the interplanetary magnetic field is not explored; our statement of openness hinges upon the tail length.) From the data it is apparent that most of the crossings of the null plane are accompanied by a residual Z component, so true nulls are rarely found. However the field does decrease which suggests that fresh field is being brought out into the tail continuously. The observation of positive and negative Z excesses further suggests that merging also occurs regularly near the null sheet. The combination indicates that the tail is often electrically active there. The geometry does not strongly favor either a substantially open or closed structure. Rather the structure near the null sheet varies from place to place, and is patchy.

Orbit 4 is most favorable for observations of the type discussed here. The regions of the orbit over which useful null crossings took place is shown in Fig. 11. The heavy lines indicate the locations of the crossings and the light backgrounds the orbit loci. Crossings are found during all parts of the outbound leg, with little correlation with

the daily wobble. However, the inbound crossings are found only near apogee. Except for variations in the direction of the solar wind, the null plane should rotate about the X axis. Thus for this time we expect a tipping of the sheet forward into the direction of planetary motion. The dusk side will be more northerly than the dawn half of the tail. Thus on the outbound leg the null sheet is favored.

The other two cases for which data is presented also display the effect that the outbound leg of the orbit samples null plane crossings more frequently than the inbound leg. Because of these effects orbit 2 shows no null crossings and orbit 3 only 20. Orbit 6 data do not provide null crossings as the spacecraft was in the transition region on the outbound leg.

Finally we report a tendency for equality of polarity distribution nearer the transition region. This is especially evident in Fig. 8 where excesses as large as 10 gamma are seen in the flanks of the tail. An increase in southward crossings with distance is also apparent in the other two cases. However, the first orbit does not reach to great distance before exiting the tail, and our conclusion does apply there.

#### THE RELATION OF $K_p$ AND THE MAGNITUDE OF THE FIELD

Behannon and Ness (1966) have reported positive correlations of increased tail field magnitude with  $K_p$ , the three-hour range planetary magnetic index. In Fig. 12 we give an example of the relation of  $K_p$  to the magnitude of the tail field. All data are at distances more than 70  $R_e$  from the center of the earth. Northern and southern hemisphere data are distinguished. By coincidence, higher  $K_p$  occurred while the spacecraft was in the southern hemisphere during the times of Fig. 12. The restricted

radial range eliminates the effect of radial gradients from the plot. Also the data is chosen to eliminate regions near the null plane to obtain a more representative view of the core of the tail in both the northern and southern hemispheres. Values of  $Z$  for this data range from  $+12.3$  to  $-13.3 R_e$ . Values of  $K_p$  encountered vary from  $0_0$  to  $6_-$ . There is a general trend to encounter higher tail fields with larger values of  $K_p$ . However, the spread of values shows that the relation is not clear. For example the largest tail magnitude here of  $\sim 20$  gamma occurred for  $K_p = 3+$  while the largest value of  $K_p = 6_-$  took place when the field was  $17$  gamma. Similar trends are evident in plots of data closer to the earth.

Cursory examination of the plot suggests that the relation connecting  $K_p$  and  $B$  is non-linear. A more linear relationship is shown in Fig. 13 where the values of  $B$  are plotted against  $a_p$ . The spread is larger as expected for a linear plot. However the dependence can only be said at this time to indicate an increase of  $B$  with magnetic activity. The values of  $a_p$  of Figure 13 have been obtained from the values of  $K_p$  of Fig. 12 using the relation given by Hirshberg (1965),  $\log a_p = 0.25K_p + 0.4$ .

#### THE RADIAL GRADIENT

The magnitude of the field in the tail varies for the data sample used between the extremes of  $4$  to  $40$  gamma. Generally the field appears to take on values more nearly from  $10$  to  $20$  gamma. These data are plotted in Fig. 14. These values are qualitatively similar to those reported previously (Ness, 1965; Ness et al., 1967; Fairfield and Ness, 1967). The values reported here correspond to radial distances from  $10$  to  $80 R_e$ , and

a definite gradient is observed. All data used in the examination of the radial gradient satisfies the test that  $K_p \leq 2+$  for the period up to 6 hours after the observations. Also one-hour averages including null plane crossings were eliminated because the change in magnetic field direction across the neutral sheet causes the average field magnitude to be reduced.

The data are averages of 1 to 10 hourly average values, depending on the amount of spacecraft radial motion during the time. No averages include times when the spacecraft radial position is different by more than 2 earth radii. The data from the northern and southern, or positive and negative pointing fields is separated according to the solid (+) and open (-) points. There is no clear distinction in the observed gradient for the two regions of space.

A weighted least-squares fit of the data of Fig. 14 to both a power law and exponential discloses little choice. The values we report for the equations are

$$|\vec{B}| \propto R^{-0.74 \pm 0.01}$$

for the power law and

$$|\vec{B}| \propto \exp\left(-\frac{R(\text{earth radii})}{59.4 \pm 0.3}\right)$$

for the exponential. The correlation coefficient between  $\ln B$  and  $\ln R$  (power law fit) is 0.865 (0.916 with the wildest point excluded). The correlation coefficient between  $\ln B$  and  $R$  (exponential fit) is 0.863 (0.914 with the wildest point excluded). The possibility that a power law is the best fit comes partly from the near earth values of the field which being high tend to bias the data upwards.

From the theoretical standpoint either law can be thought to apply depending upon the model chosen. For example if the tail is assumed to

essentially be free of field annihilation then any expansion as the distance from earth increases would follow a power law dependence. On the other hand loss of field with a rate proportional to the field intensity should be exponential, i.e. first order. This latter statement would be based upon the simple case where the system is adiabatic and all energy lost in the field would be transferred to the plasma so that the pressure is constant.

The amount of data provided by the first few orbits is insufficient to establish without doubt the existence of components of gradient in the directions Y or Z. It was deemed advisable to study this question within the constraints of the data in order to determine whether the radial gradient was contaminated. The reason for possible contamination is that the orbits vary with respect to all three coordinates and therefore some distinction is required. We show in Figs. 15, 16 and 17 the cross gradients taken under the constraints stated. These data are taken from a mixture of orbits; the criterion is that the radial distance from earth be held to a small tolerance compared to the total scale of the effects being studied. Therefore, data from different  $10 R_e$  segments of radial distance is considered separately. There appears a tendency in Figs. 15 and 16 for the dusk edge fields to be smaller. The following analysis indicates that any such effect apart from a radial gradient is not statistically significant. This apparent effect is not seen in the case of the transverse studies for  $R > 70 R_e$ . As all these data are in the solar-magnetospheric system it does not appear likely that the apparent gradients are due to coordinate effects; if they were, the effect should increase with distance where the solar wind would influence the tail geometry more.

A four variable multiple correlation analysis was performed on 708 separate hourly averaged geomagnetic tail field measurements. The 708 values are all available from Explorer 33 in 1966. They include the data of Fig. 14 and corresponding data, for  $K_p > 2+$ , but exclude all neutral sheet crossings. The analysis produces regression and correlation coefficients, given in Table 1, for a least squares fit of the 708 hourly averaged values to  $B = A - m \ln R + b a_p + C |Y| + D |Z|$ , where the multiple correlation coefficient of B, the field magnitude, with the four variables R,  $a_p$ ,  $|Y|$  and  $|Z|$  is 0.801.

Table 1. Results of multiple correlation analysis of tail field magnitudes

<u>Regression coefficients</u>	<u>Partial correlation coefficients</u>
A = 47.1	-----
m = 9.12	rBR•aYZ = 0.800
b = 0.186	rBa•RYZ = 0.413
C = -0.0772	rBY•RaZ = 0.148
D = -0.0159	rBZ•RaY = 0.062

R is the geocentric radial distance and  $|Y|$  and  $|Z|$  are the absolute values of the transverse, solar-magnetospheric position coordinates. The values of  $a_p$  are obtained using the relation given by Hirshberg (1965). The regression and correlation coefficients are given in Table 1. The units of B are  $\gamma$ ; the units of R,  $|Y|$  and  $|Z|$  are earth radii. The correlation coefficient of B with the three variables  $a_p$ ,  $|Y|$  and  $|Z|$  alone is 0.444. The radial dependence alone from this multiple correlation analysis,  $B = 47.08 - 9.119 \ln R$ , is plotted on Fig. 14, together with the results of power law and exponential fits to the data for  $K_p \leq 2+$  only.

The multiple correlation result has almost as high correlation as the other two.

The small values of  $r_{BY \cdot RaZ}$  and  $r_{BZ \cdot RaY}$  on Table 1 show these tail field magnitudes are not significantly correlated with  $|Y|$  and  $|Z|$ .

Murayama (1966) has analyzed Explorer 18 (IMP 1) energetic electron data in the geomagnetic tail, using the distance from the neutral sheet,  $Z_n$ , as an independent variable. The regression and partial correlation coefficients for the Explorer 33 tail field magnitudes using  $Z_n$  are  $D_{Z_n} = -0.0132$  and  $r_{BZ_n \cdot aY} = 0.0519$ , which also is not a significant correlation.

The small, non-significant value of  $r_{BY \cdot RaZ}$ , a measure of the dependence of B on  $|Y|$  alone, indicates the tail field magnitudes are uniformly distributed transverse to the tail axis, when the radial gradient and effects of geomagnetic activity are considered. This suggests the tail field magnitudes on either the dusk or dawn sides are fairly uniform out to the tail boundary. The suggestion from Figs. 15 and 16 that the magnitudes are smaller near the boundary does not appear from a multiple correlation analysis which includes the effect of solely radial gradients. Since the value of  $r_{BZ \cdot RaY}$  is even smaller than that of  $r_{BY \cdot RaZ}$ , this analysis gives no evidence for a general depression of tail field magnitude within  $5 R_e$  of the null sheet ( $|Z|$  or  $|Z_n| \sim 0$ ) as reported by Anderson and Ness (1966) from Explorer 18 (IMP 1) data. (The null sheet, inferred by Speiser and Ness (1967) to be  $\sim 10^3$  km thick, is an exception.)

#### EXTENSION OF THE TAIL FIELD TO GREAT DISTANCE

The present series of measurements of magnetic field extend the ordered tail field beyond lunar distance and to the apogee of the orbit,

i.e.  $82 R_e$ . This finding is in substantial agreement with that reported by Ness et al. (1967) from another magnetometer experiment aboard the same spacecraft. Further extension of tail configuration is suggested by Wolfe et al. (1967) from measurements of plasma at  $\sim 10^3 R_e$  from the earth. These latter measurements from Pioneer 7 disclose a fluctuating structure suggesting a magnetic wake. At the present time the Explorer measurements represent the greatest penetration into nominally ordered tail fields. It appears likely that these measurements do not represent a terminus for the ordered tail.

As shown on Fig. 1, the earth's orbital motion sweeps the satellite apogee through the tail, which permits the extent of the tail at apogee to be found. The exact value must await further refinement of the crossings of the satellite through the magnetopause as the measurements are disturbed by fluctuation phenomena. However the ordered fields of the tail extend some  $20 R_e$  on the dusk and dawn sides though detailed examination may disclose some differences later. These results are seen in Figs. 6 and 7 which show composite presentations of all 1966 tail data projected into the ecliptic plane. The moon should be immersed in the tail for some  $\pm 15$  degrees to either side of the X axis, or for 8.3% of its orbital period.

Russian measurements appear to have disclosed a region of perturbed field and plasma near the lunar surface (Gringauz et al., 1966). Sufficient detail is not available to recognize these measurements as associated with the earth's magnetic tail, though Ness (1967) has pointed out that these data are not typical of an interaction with the solar wind (the moon was immersed in the tail at the time of the observations).

### THE LUNAR INTERACTION WITH THE TAIL

The primary effects of the immersion of the moon in the tail field is the turnoff of the streaming solar wind and the change in the magnetic field amplitude and direction. The relative motion is now determined by the motion of the moon against the plasma in the tail. For simplicity we assume that the tail plasma has zero bulk velocity. Then the relative motion is given by the orbital motion of the moon about the earth,  $\sim 1.0 \text{ km sec}^{-1}$ . The magnetic field changes from the idealized spiral angle of 45 degrees to either parallel or antiparallel to the direction from the sun. The magnitude increases from the nominal value of 5 gamma for the interplanetary field to as high as 15 gamma for the tail field at the distance of the moon.

When exposed to the direct solar wind with nominal parameters of  $400 \text{ km sec}^{-1}$  bulk velocity and a magnetic field as quoted, the free stream motional electric field is  $2 \times 10^{-3} \text{ volts m}^{-1}$ . The interaction with the moon is governed by the internal intrinsic electrical conductivity, and by the assumption that whatever plasma strikes the lunar surface is totally adsorbed, neutralized and re-emitted thermally, following the magnetospheric model of Gold (1966). In the model of Sonett and Colburn (1967) the moon functions as a unipolar generator with the solar wind supplying the brush action. If we assume cylindrical symmetry, it is possible to compute the total planetary current flowing in the mode described by solutions to the fundamental equation for the interior potential which are expressed by Legendre polynomials. For the  $P_1$  mode and a radiogenically hot moon in the free solar wind, the total current in the  $P_1$  mode is limited to  $\sim 10^5$  amperes.

The same reasoning applied to the steady state when the moon is immersed in the tail field, yields a motional electric field for a stationary tail  $\sim 10^{-5}$  volts  $m^{-1}$  and the planetary  $P_1$  current system is reduced by two orders. In this case the interaction is characterized as weak. Also the formation of a shock wave is inhibited; the largest wave would be infinitesimal.

The conditions leading to the immersion in the tail field as a steady state condition require substitution of a Cowling current system for the unipolar current. This case is valid during the transfer from interplanetary to tail or the reverse. During the transition, which is expected to take an appreciable time due to the general diffuseness of the magnetopause, the field would fluctuate and the plasma would alternately be that of the transition region and the tail. Then the current systems would be determined by electromagnetic induction to which the Cowling decay time applies. However even for a relatively conducting moon, and if the conductivity were associated with a high temperature so that the magnetic permeability were near the free space value, the "diffusion" time for the magnetic field is hardly more than  $10^2$  sec.

A more subtle condition arises from the instance when the orbit of the moon intersects the null plane, for then the key parameter for the establishment of the unipolar system is also the Cowling constant. However even here the new conditions will be established in a time short to most relevant times. However in the special circumstance that the null intersects the moon for an extended period of time, it is clear that the current system which is established in the steady state is a complicated modification of the simple unipolar one.

In the case of the intersection with the null which is long lasting, the maximum electric field is established across the null plane because of the field reversal. Unless the symmetry is such that the null intersects the moon on its equator, even the  $P_1$  current system is modified. For electrically reasonable moons, the interaction is so weak that the loss factor,  $k$ , representing field and plasma slipping to the flanks of the moon, approaches zero. The null intersection with the moon must reverse the direction of the electric field. This means that a region of charge must be established in the interior, and even for the uniform moon, the electric field in the interior is no longer uniform. The sense of the charges deposited in the interior depends upon the directions assumed by the fields.

## FIGURE TITLES

- Fig. 1. Projections into the plane of the ecliptic and normal containing the earth-sun line of the first 11 orbits of Explorer 33 during July to December 1966. The first and eleventh orbits clearly show the effects of perturbations by the moon during close approach of the spacecraft.
- Fig. 2. Block diagram of the magnetometer subsystem of the Ames instrument, showing driver, detector, and feedback blocks.
- Fig. 3. Block diagram of the complete magnetometer including spin demodulators.
- Fig. 4. Examples of geomagnetic tail data averaged over different time intervals and by the two procedures described in the text corresponding to component and magnitude averages. Each of the three cases is a time series of the average value of the field magnitude. C indicates magnitude average and I the average obtained by averaging of the components. The difference in the magnitude is shown in the ordinate for each of the three cases.
- Fig. 5. Examples of the error in the averaged field for the geomagnetic tail using the component method compared to the magnitude method. The number of minutes per average is shown in the abscissa. The inclusion of null crossings is shown to significantly influence the value of the magnitude.
- Fig. 6. Projections on the solar magnetospheric X-Y plane of three-hour-average magnetic field vectors measured in the earth's magnetic tail. The data are from orbits 1, 4, 5, 6, 7 and 8 of Explorer 33, and were

taken at times during July 1 to November 10, 1966 when the spacecraft was in the southern half of the tail. The averages are obtained by magnitude averages and the directions by component averages.

Fig. 7. Projections on the solar-magnetospheric X-Y plane of three-hour-average magnetic field vectors measured in the earth's magnetic tail. The data are from orbits 2, 3 and 4 of Explorer 33 and were taken at times during July 14 to August 26, 1966 when the spacecraft was in the northern half of the tail. The method of averaging is the same as for Fig. 6.

Fig. 8. Z-component of magnetic field at neutral sheet crossings (when X-component reverses sign) during orbit 1 of Explorer 33. A tentative location of the magnetopause is indicated by a dashed line. The segment is approximately 36 hours long. The location of the spacecraft in solar magnetospheric coordinates is given at the bottom of the graph.

Fig. 9. Z-component of magnetic field at neutral sheet crossings (when X-component reverses sign) during orbit 5 of Explorer 33. The location of the magnetopause is indicated.

Fig. 10. Idealized meridian plane representation of the formation of loops of magnetic field near the neutral sheet in the geomagnetic tail by severing and reconnection. The neutral sheet is indicated by a shaded band. The longitudinal extent of the loops may be limited. This model is suggested by the discovery of both northward and southward Z residuals where the X component of field reverses sign.

Fig. 11. Plan and elevation view of orbit 4 of Explorer 33 in solar magnetospheric coordinates. Heavy portions of the orbit trace

indicate where neutral sheet crossings (reversals of sign of X-component of magnetic field) occur. One day marks are given on the orbit traces. The sign of the X-component of the field is generally positive before 1104 UT on August 22 and generally negative afterwards.

Fig. 12. 1966 Explorer 33 one hour average geomagnetic tail field magnitudes with the component of the spacecraft location along the earth-sun line, X, more than 70 earth radii behind the earth, plotted against  $K_p$ . The dots indicate anti-solar oriented field vectors (southern hemisphere); the crosses indicate solar oriented field vectors (northern hemisphere). The number of individual magnetic field samples averaged during each one hour period ranges from 331 to 587.

Fig. 13. The data of Fig. 12 replotted against  $a_p$ , without designation of field polarity.

Fig. 14. 1966 Explorer 33 hourly average geomagnetic tail field magnitudes with hours excluded during which sheet crossings occur. Symbols indicate the number of hourly averages used for each point. Solid symbols indicate solar-directed (northern hemisphere) fields; open symbols are for anti-solar directed (southern hemisphere) fields. Data suggesting a decrease in field magnitude near the edges of the tail (not necessarily near the neutral sheet) have been deleted. Weighted least-squares fit to the data, assuming exponential and power law dependences, are given. The expression  $B = 47.1 - 9.12 \ln R$ , which is a result from a multiple correlation analysis using tail field magnitudes for all values of  $K_p$ , is also presented.

Fig. 15. 1966 Explorer 33 hourly average geomagnetic tail field magnitudes for geocentric distances between 30 and 40 earth radii, plotted against the transverse coordinates, Y and Z. Hourly averages during which sheet crossings occur have been excluded. The dots indicate anti-solar directed (southern hemisphere) fields; the crosses indicate solar directed (northern hemisphere) fields.

Fig. 16. Same as Fig. 15 but for geocentric distances between 40 and 50 earth radii.

Fig. 17. Same as Fig. 15 and Fig. 16 but for the component of spacecraft location along the earth-sun line, X, more than 70 earth radii behind the earth.

## REFERENCES

- Anderson, K. A., Energetic electron fluxes in the tail of the geomagnetic field, J. Geophys. Res., 70, 4741-4763, 1965.
- Anderson, K. A., and N. F. Ness, Correlation of magnetic fields and energetic electrons on the IMP 1 satellite, J. Geophys. Res., 71, 3705-3727, 1966.
- Axford, W. I., H. E. Petschek, and G. L. Siscoe, Tail of the magnetosphere, J. Geophys. Res., 70, 1231-1236, 1965.
- Bame, S. J., J. R. Asbridge, H. E. Felthausen, E. W. Hones, and I. B. Strong, Characteristics of the plasma sheet in the earth's magnetotail, J. Geophys. Res., 72, 113-129, 1967.
- Behannon, K. W., and N. F. Ness, Magnetic storms in the earth's magnetic tail, J. Geophys. Res., 71, 2327-2352, 1966.
- Coppi, B., G. Laval, and R. Pellat, Dynamics of the geomagnetic tail, Phys. Rev. Letters, 16, 1207-1210, 1966.
- Dessler, A. J., and R. D. Juday, Configuration of auroral radiation in space, Planet. Space Sci., 13, 63-72, 1965.
- Fairfield, D. H., and N. F. Ness, Magnetic field measurements with the IMP 2 satellite, J. Geophys. Res., 72, 2379-2402, 1967.
- Gold, T., The magnetosphere of the moon, in The Solar Wind, edited by R. J. Mackin, Jr., and M. Neugebauer, Pergamon Press, 1966.
- Gringauz, K. I., V. V. Bezrukikh, M. Z. Khokhlov, L. S. Musatov, and A. P. Remizov, Signs of crossing by the moon of the earth's magnetosphere tail according to data of charged particle traps on the first artificial satellite of the moon (Luna - 10), Doklady A.N.SSSR,

- Geophysics Series, 170, 570-573, 1966 (NASA-Goddard Space Flight Center Translation No. ST-PF-LPS-10529, October 27, 1966).
- Hirshberg, J., A comparison of the different empirical relationships that have been suggested between surface magnetic indices and solar wind velocities, J. Geophys. Res., 70, 3229-3230, 1965.
- Johnson, F. S., The gross character of the geomagnetic field in the solar wind, J. Geophys. Res., 65, 3049-3051, 1960.
- Montgomery, M. D., S. Singer, J. P. Conner, and E. E. Stogsdill, Spatial distribution, energy spectra and time variations of energetic electrons ( $E > 50$  kev) at 17.7 earth radii, Phys. Rev. Letters, 14, 209-213, 1965.
- Murayama, T., Spatial distribution of energetic electrons in the geomagnetic tail, J. Geophys. Res., 71, 5547-5557, 1966.
- Ness, N. F., The earth's magnetic tail, J. Geophys. Res., 70, 2989-3005, 1965.
- Ness, N. F., K. W. Behannon, S. C. Cantarano, and C. S. Scarce, Observations of the earth's magnetic tail and neutral sheet at 510,000 kilometers by Explorer 33, J. Geophys. Res., 72, 927-933, 1967.
- Sonett, C. P., Modulation and sampling of hydromagnetic radiation, Space Res., 6, 280-322, 1966.
- Sonett, C. P., and D. S. Colburn, Establishment of a lunar unipolar generator and associated shock and wake by the solar wind, submitted to J. Geophys. Res., 1967.
- Speiser, T. W., and N. F. Ness, The neutral sheet in the geomagnetic tail: its motion, equivalent currents, and field line connection through it, J. Geophys. Res., 72, 131-141, 1967.

Wolfe, J. H., R. W. Silva, D. D. McKibbin, and R. H. Mason, Preliminary observations of a geomagnetospheric wake at 1000 earth radii, to be published in J. Geophys. Res., 1967.

Added Note:

Bame, S. J., J. R. Asbridge, H. E. Felthouser, R. A. Olson, and I. B. Strong, Electrons in the plasma sheet in the earth's magnetic tail, Phys. Rev. Letters, 16, 138-142, 1966.

Fredricks, R. W., E. W. Greenstadt, and C. P. Sonett, Magnetodynamically induced ambiguity in the data from tilted, spinning fluxgate magnetometers: Possible application to IMP 1, J. Geophys. Res., 72, 367-382, 1967.

Piddington, J. H., Geomagnetic storm theory, J. Geophys. Res., 65, 93-106, 1960.

Ness, N. F., Remarks on the interpretation of Lunik 10 magnetometer results, Goddard Space Flight Center Report X-612-67-9, January, 1967 (published in Geomagnetism i Aeronomiza, 7, No. 3, (1967)).

## ACKNOWLEDGEMENTS

The author wish to express their appreciation to the AIMP Project Office at NASA Goddard Space Flight Center, Mr. Paul G. Marcotte and his staff, for their considerable support in carrying out the experiment, and to the Honeywell Radiation Center, especially D. Longland, B. Pearlstein and D. Monisette. We also thank Mrs. Jerre McCulley and staff for critical assistance for programming in data reduction.

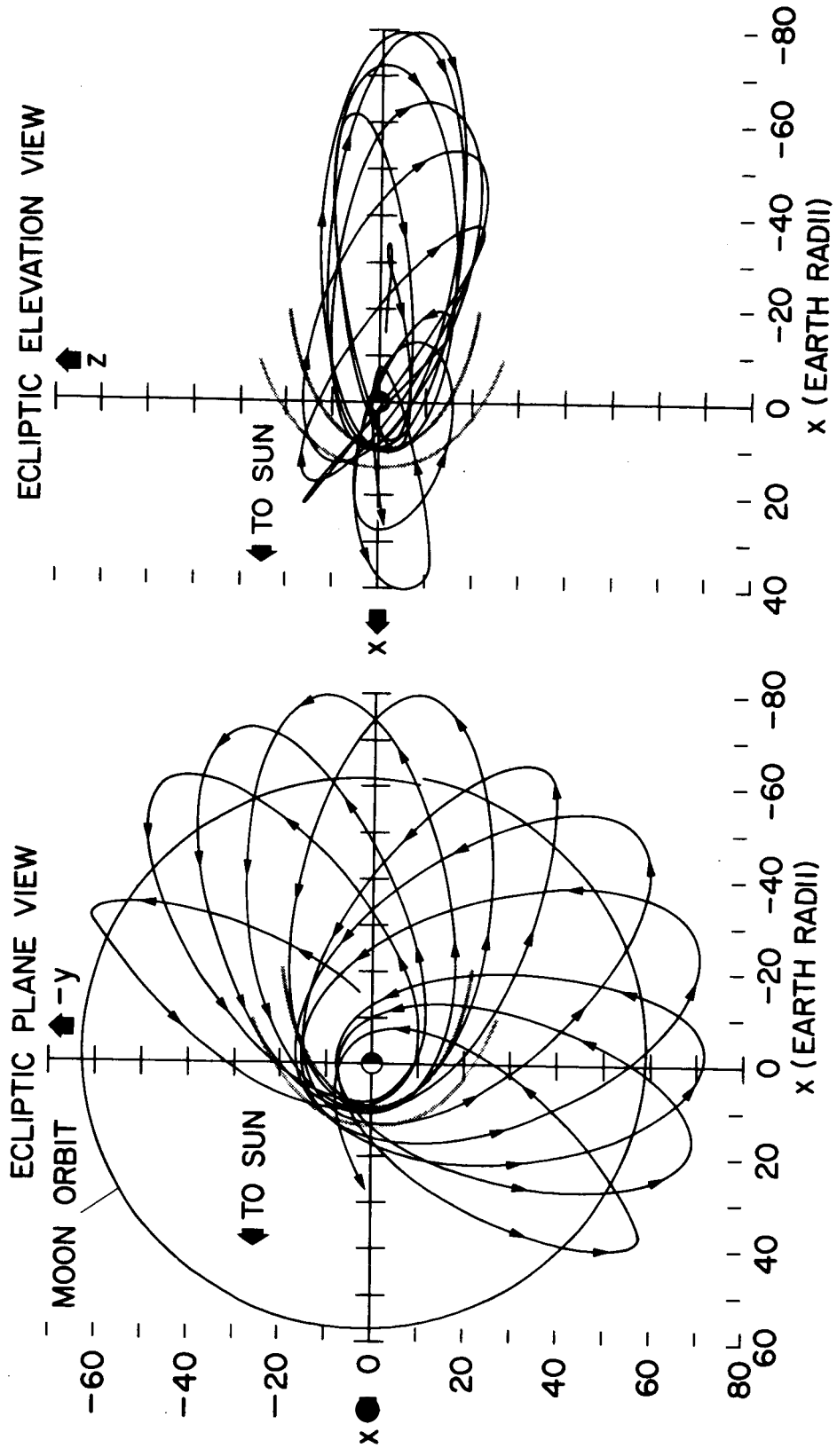


Fig. 1

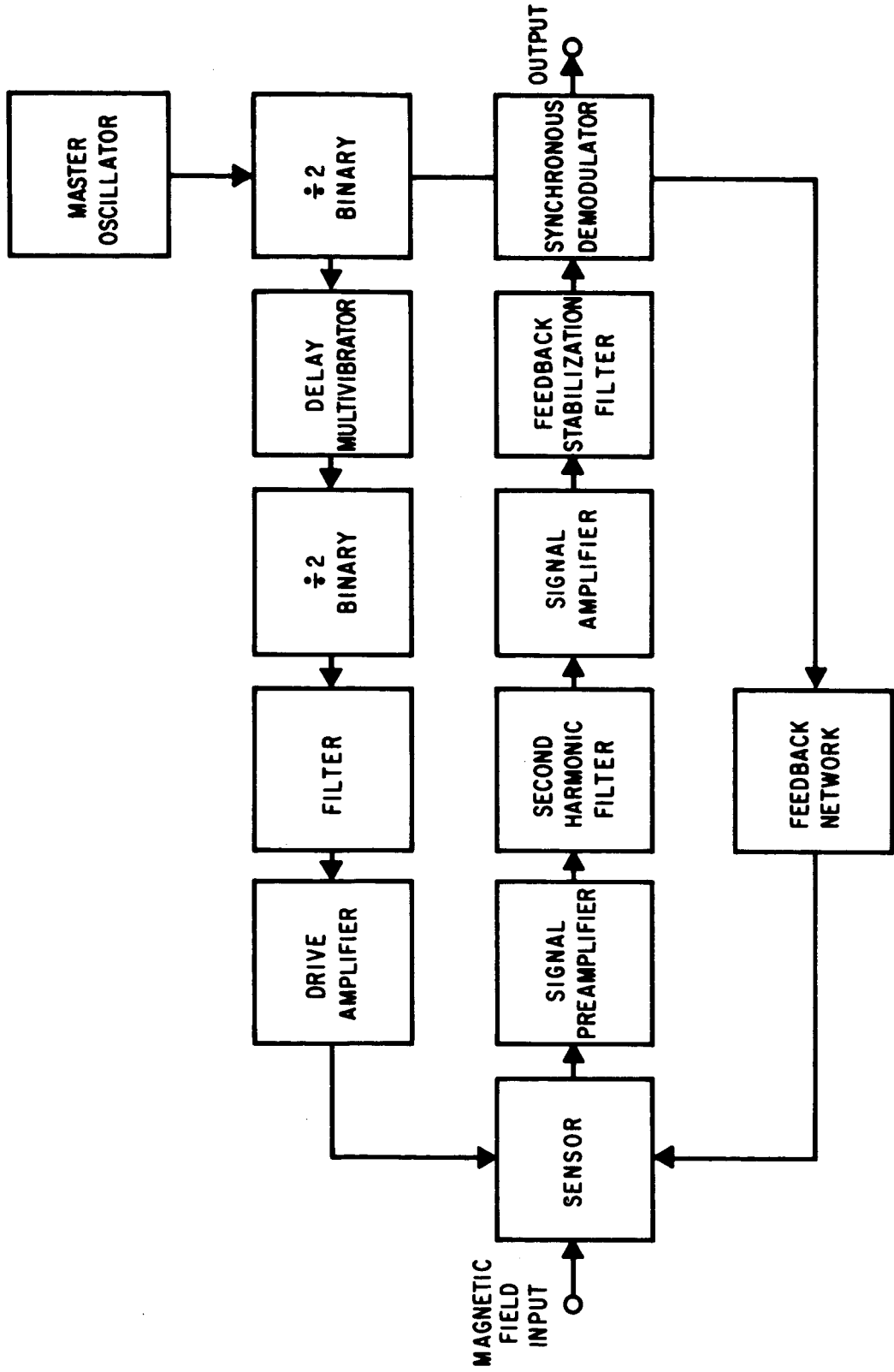


Fig. 2



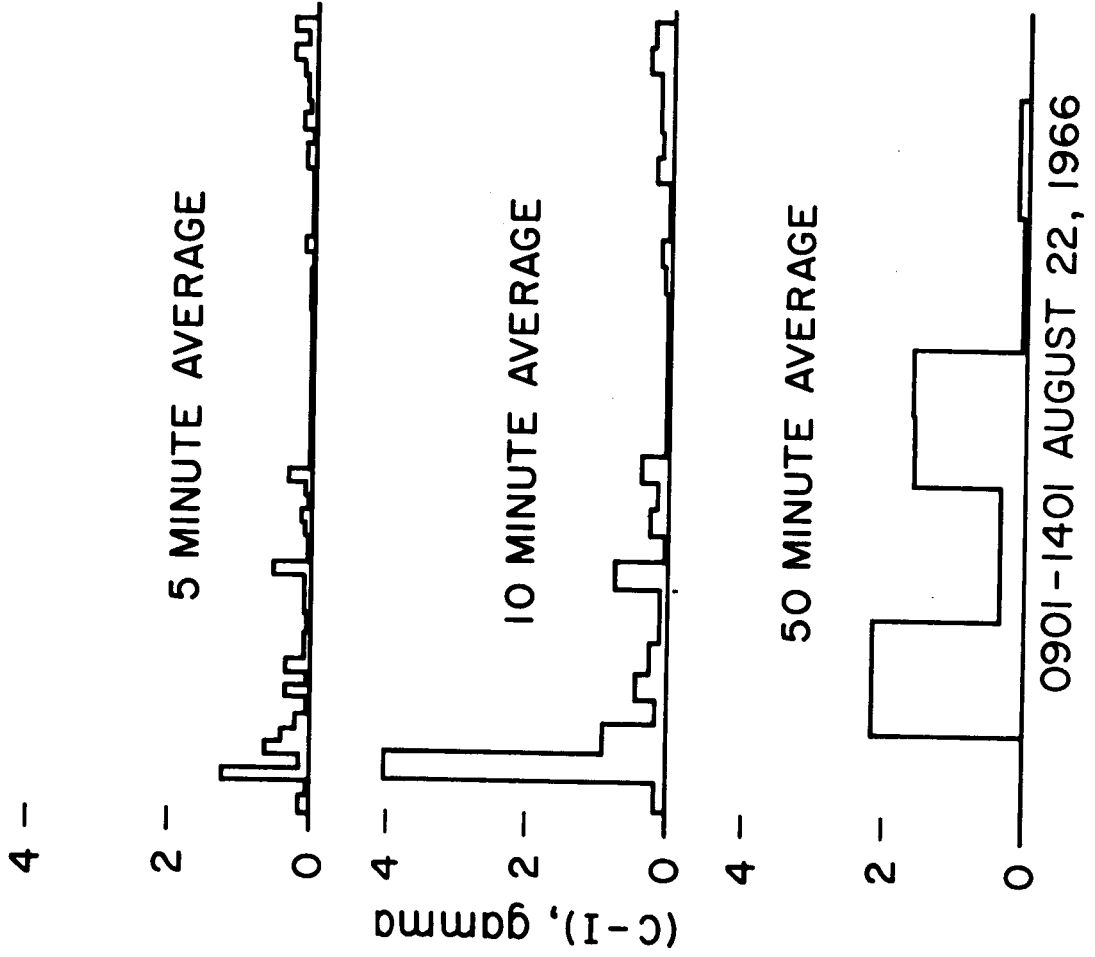


Fig. 4

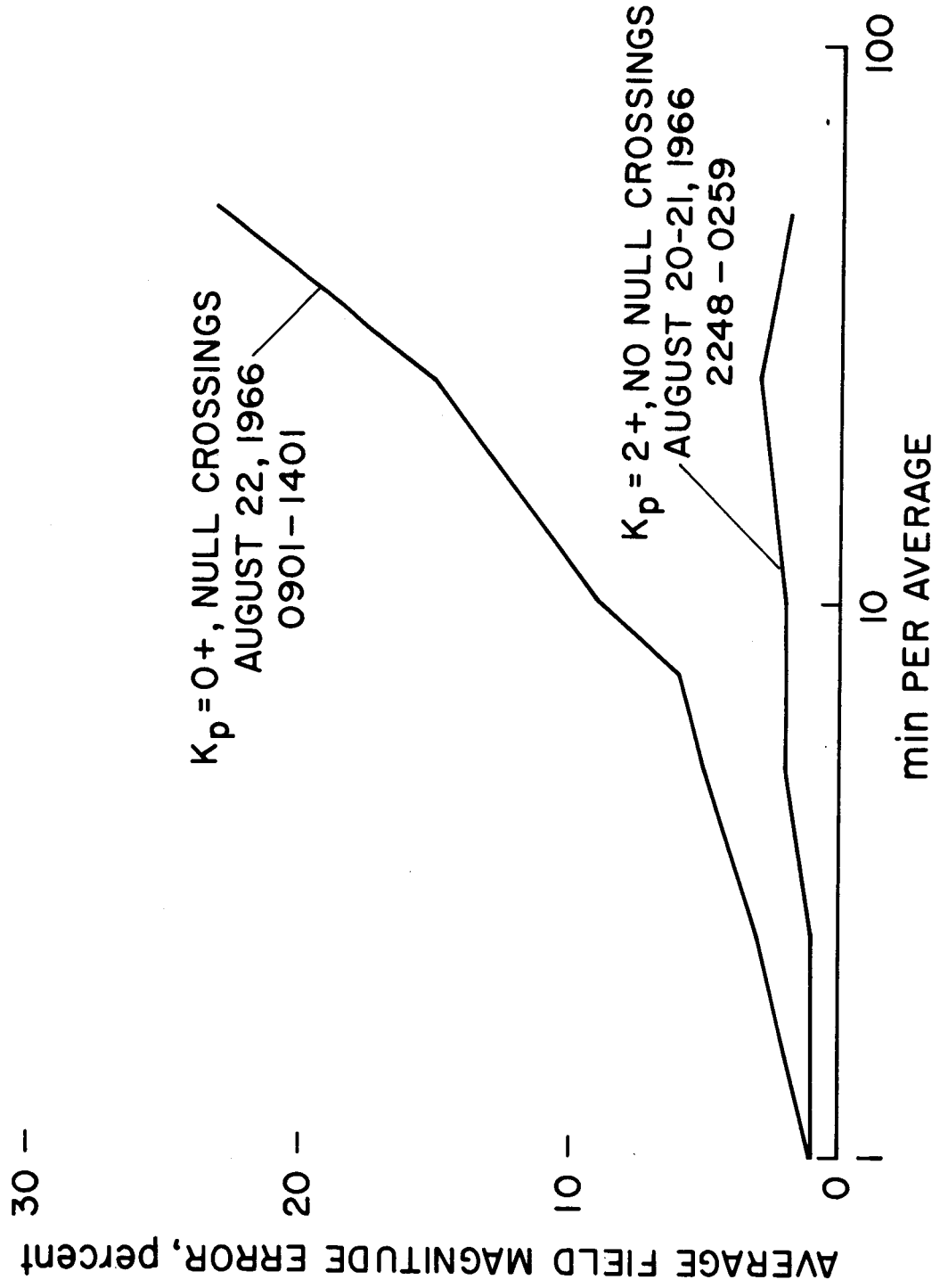


Fig. 5

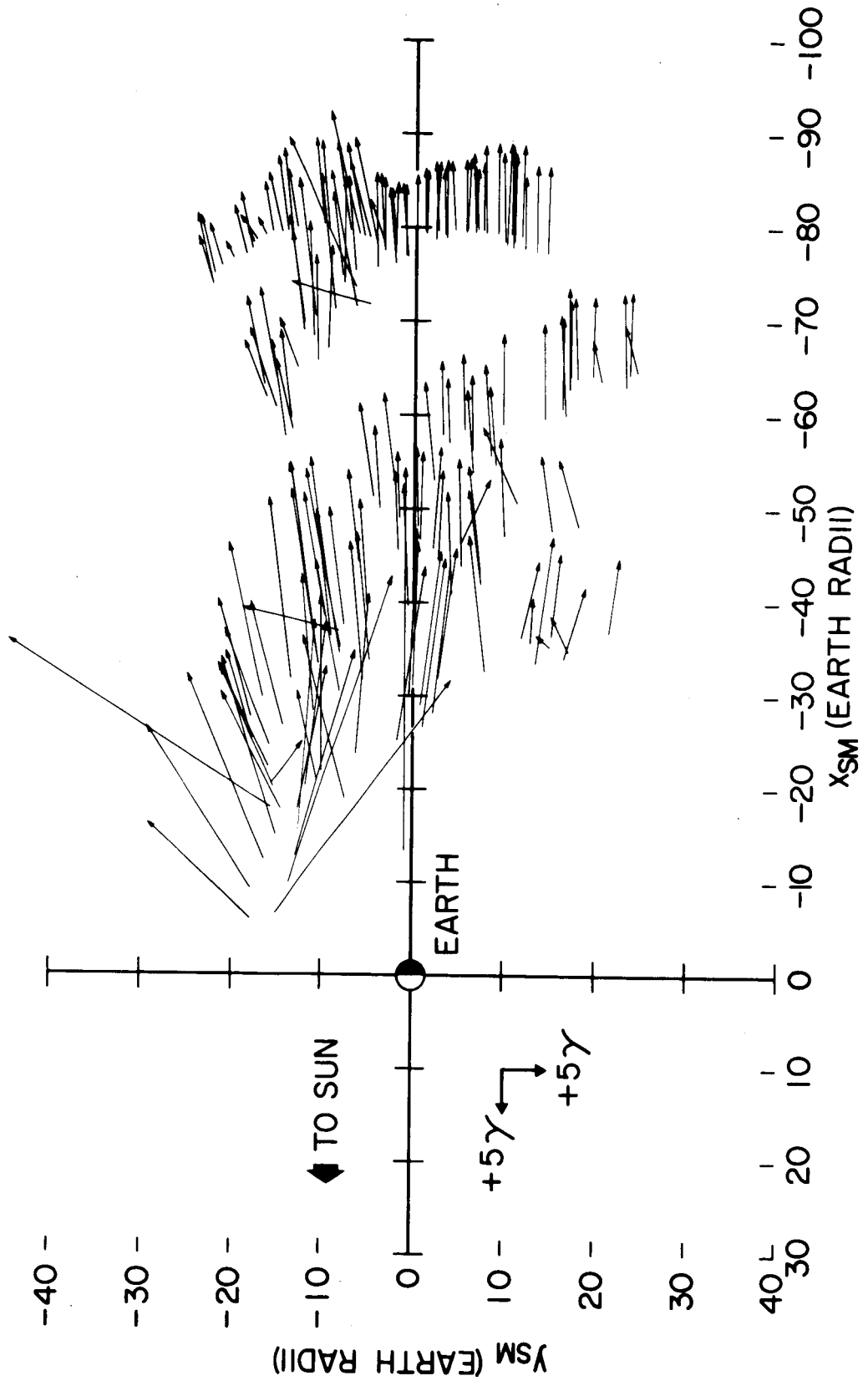


Fig. 6

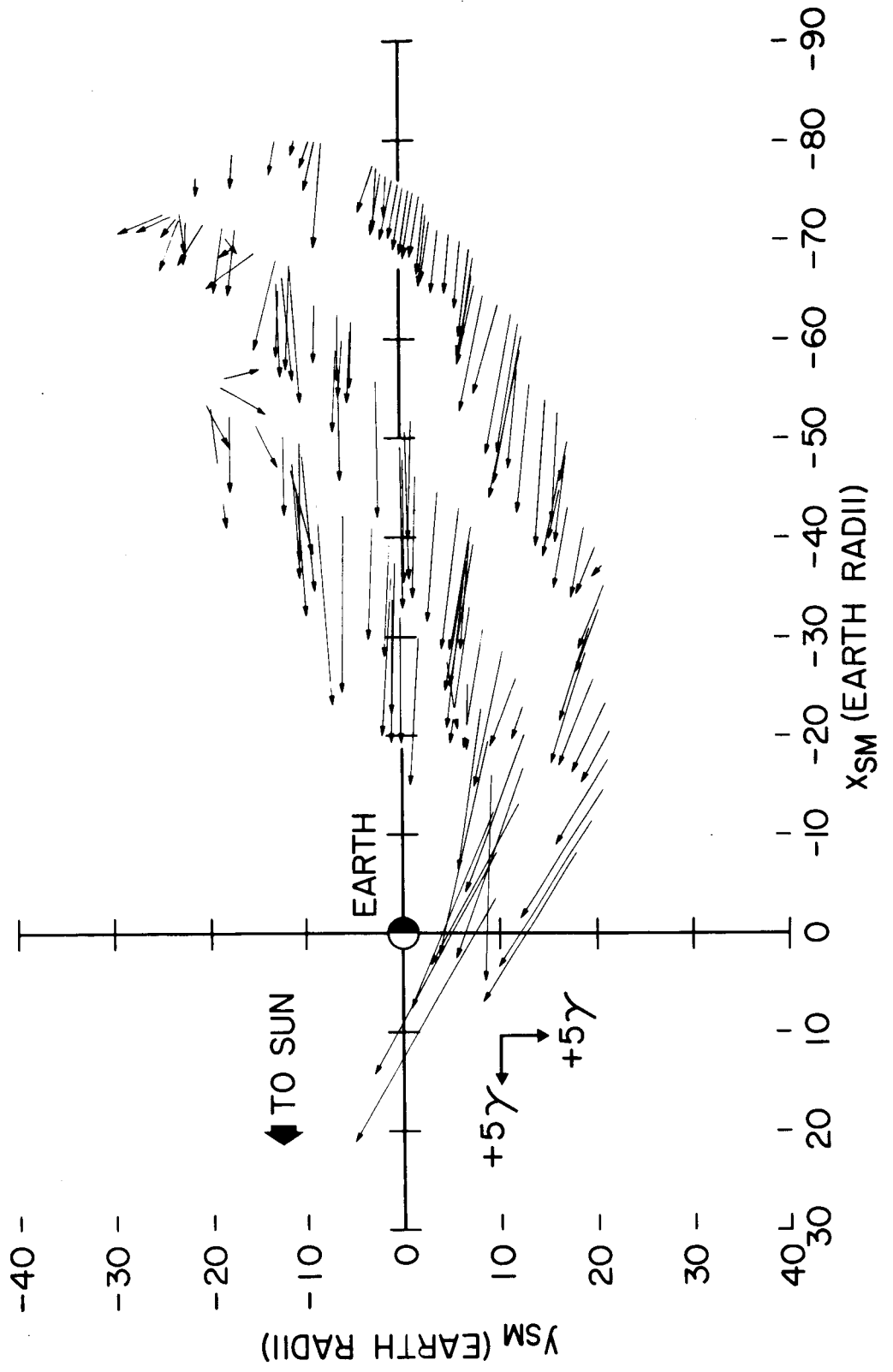


Fig. 7

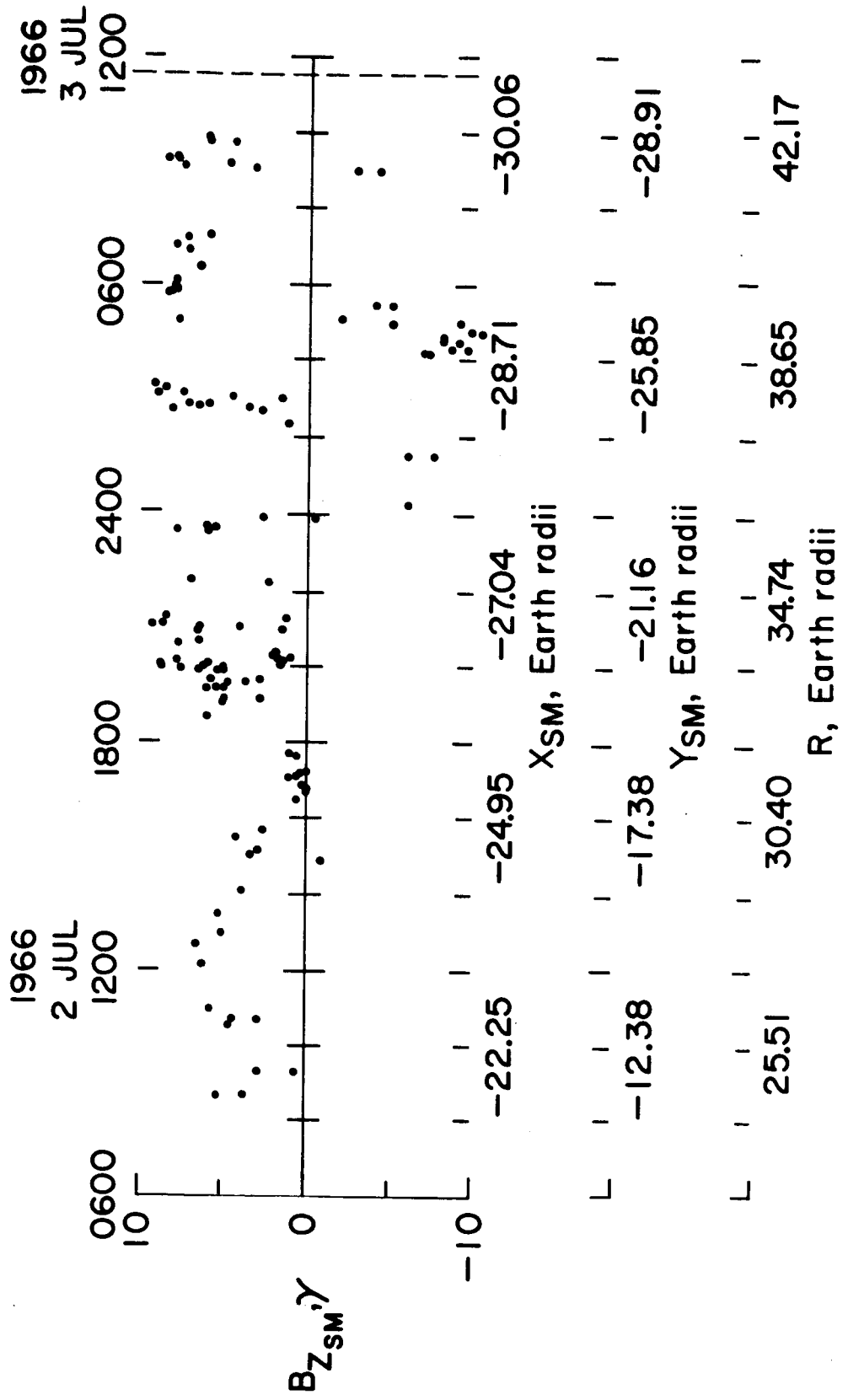


Fig. 8

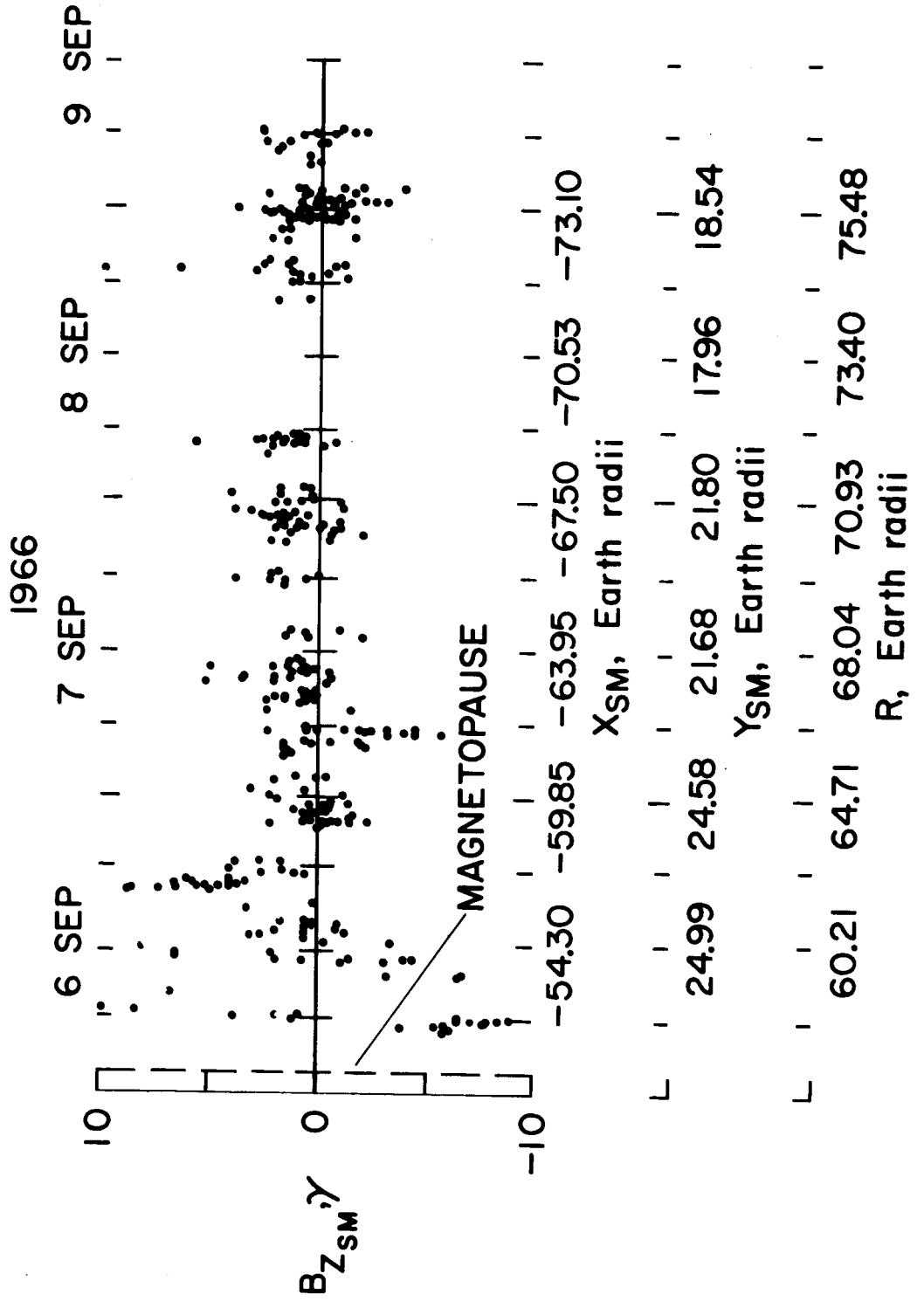


Fig. 9

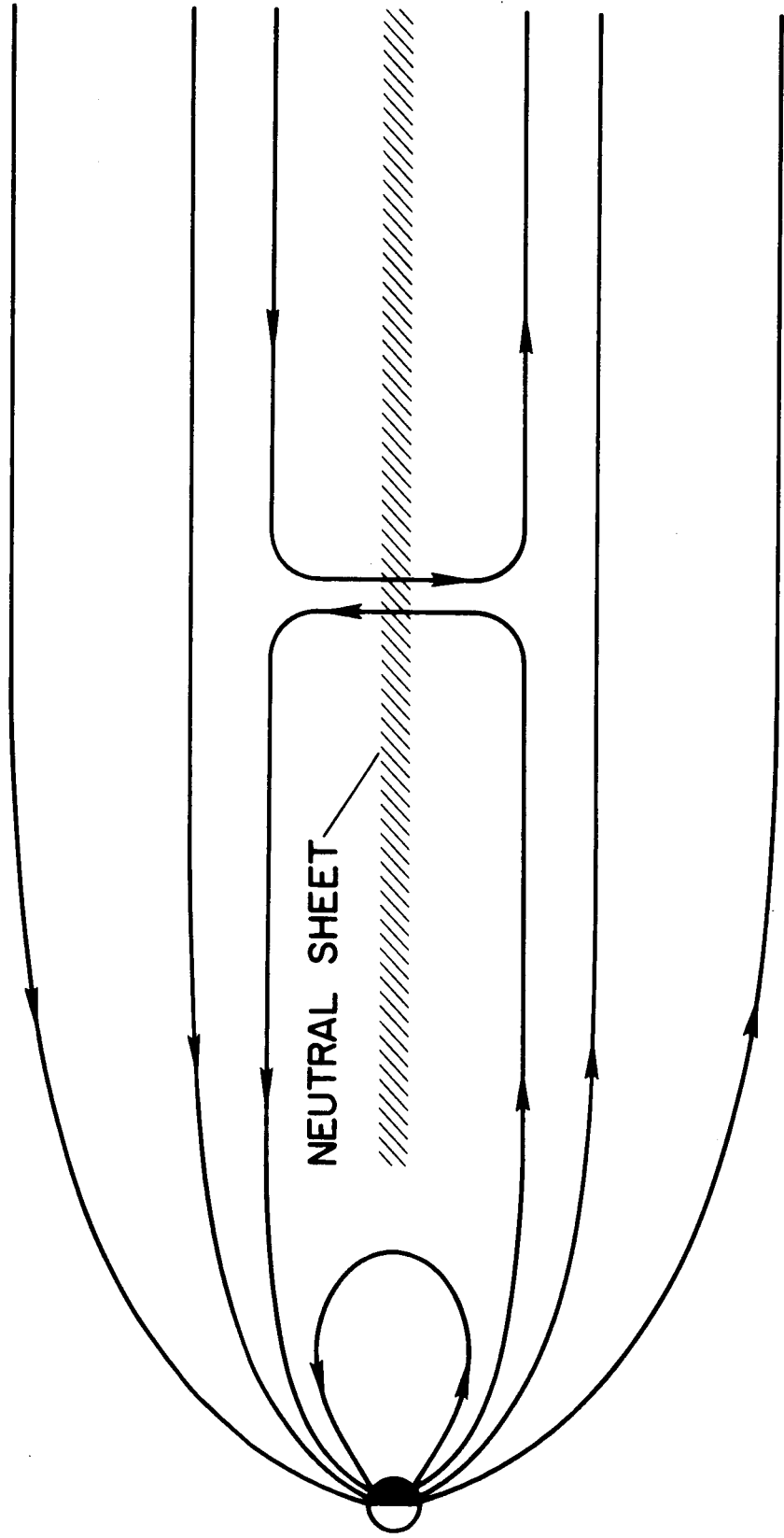


Fig. 10

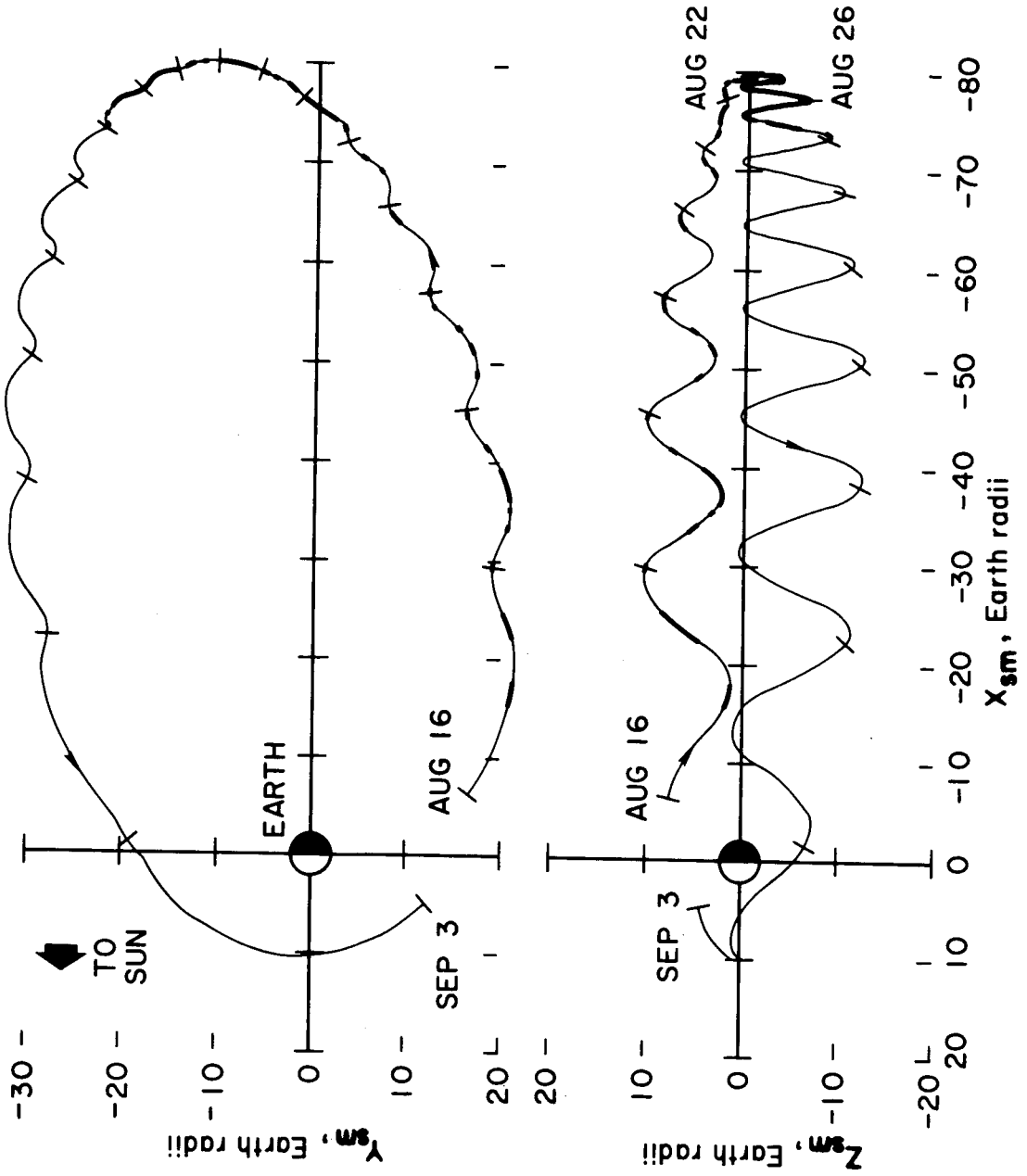


Fig. 11

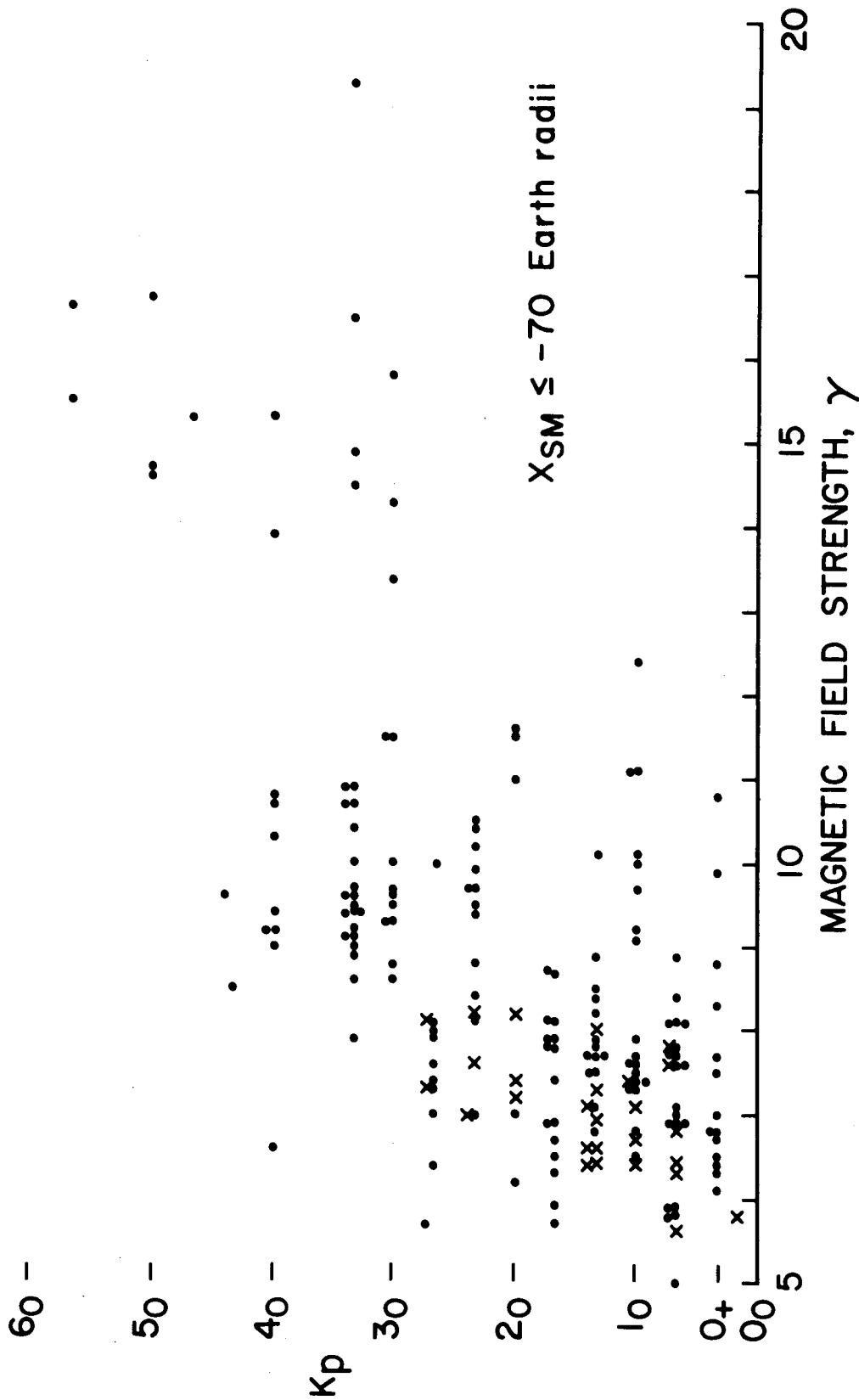


Fig. 12

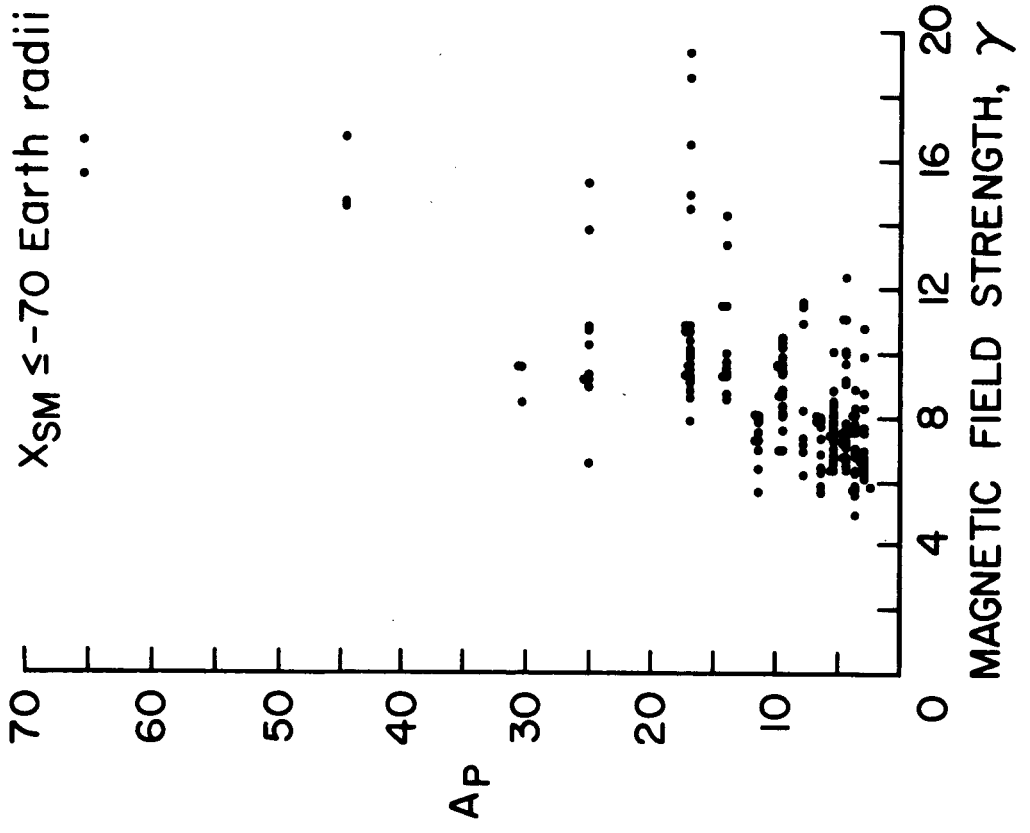


Fig. 13

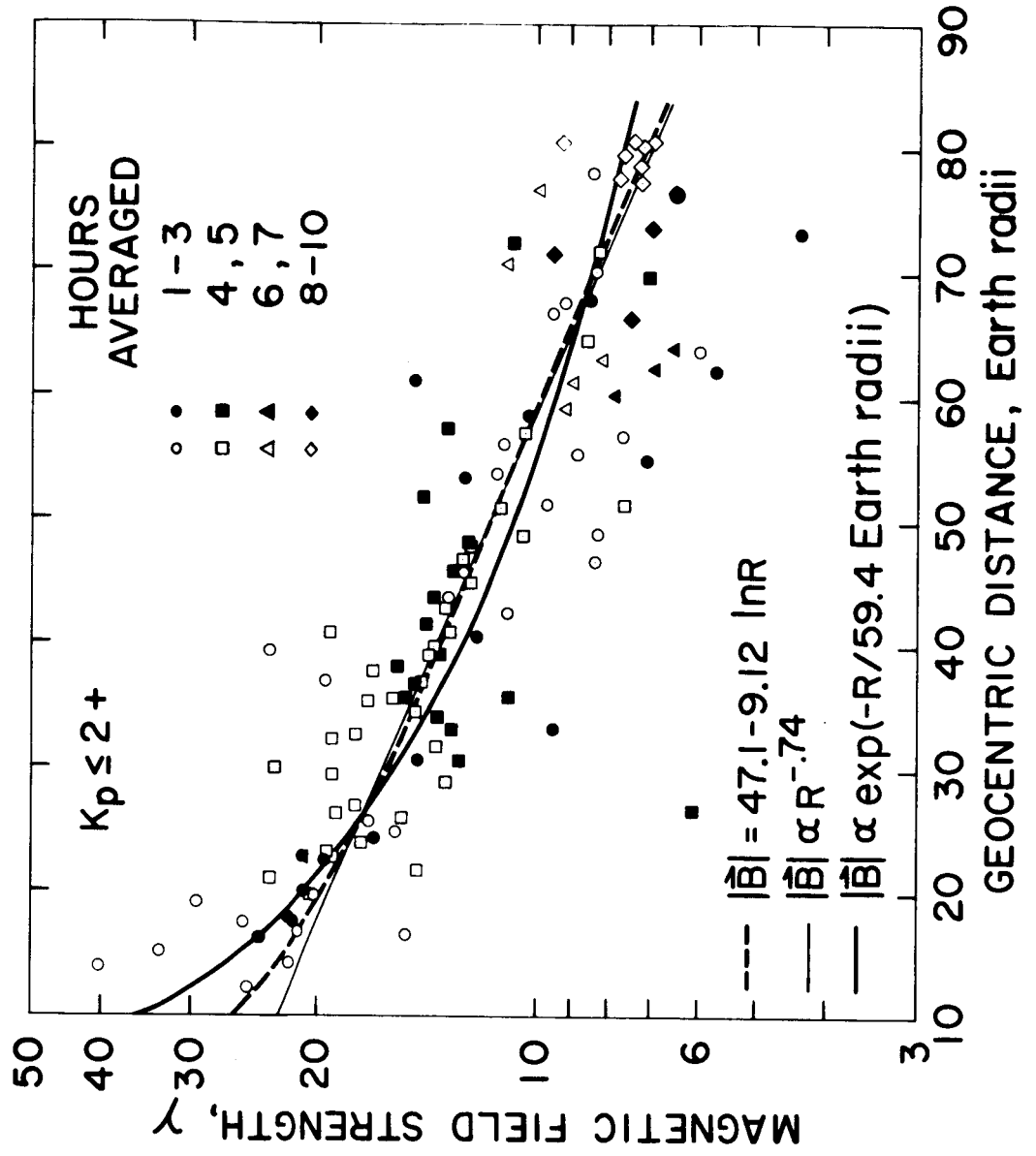


Fig. 14

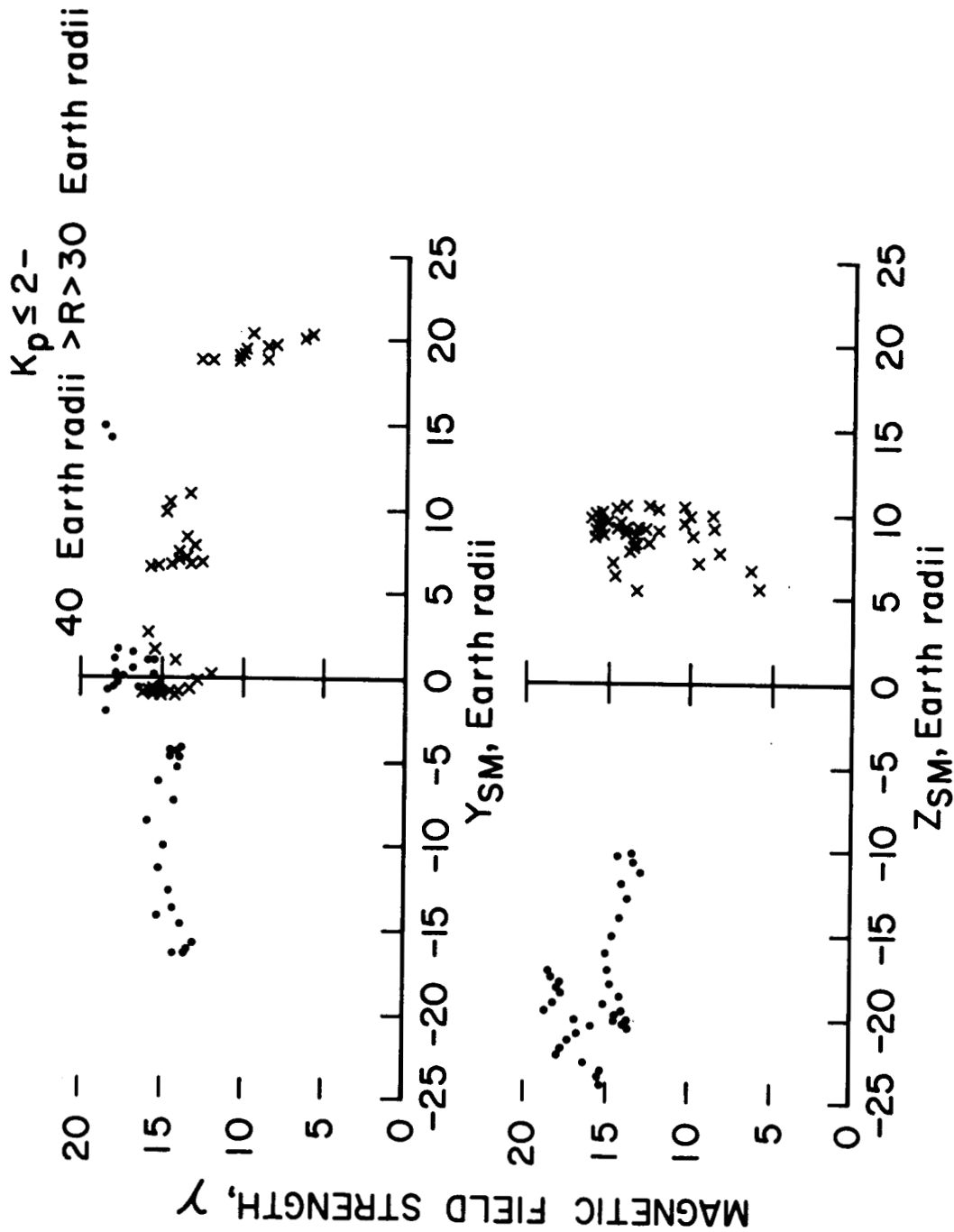


Fig. 15

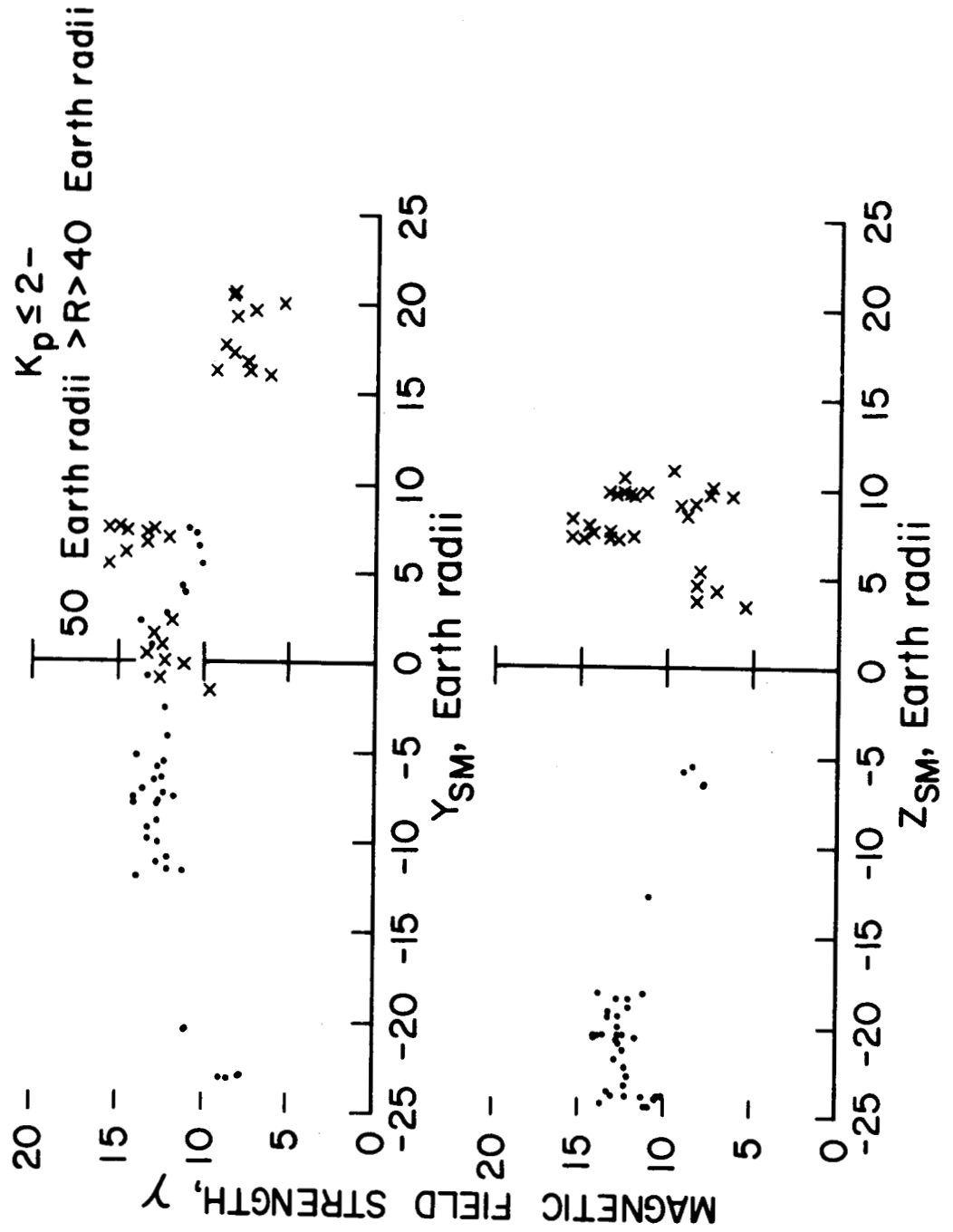


Fig. 16

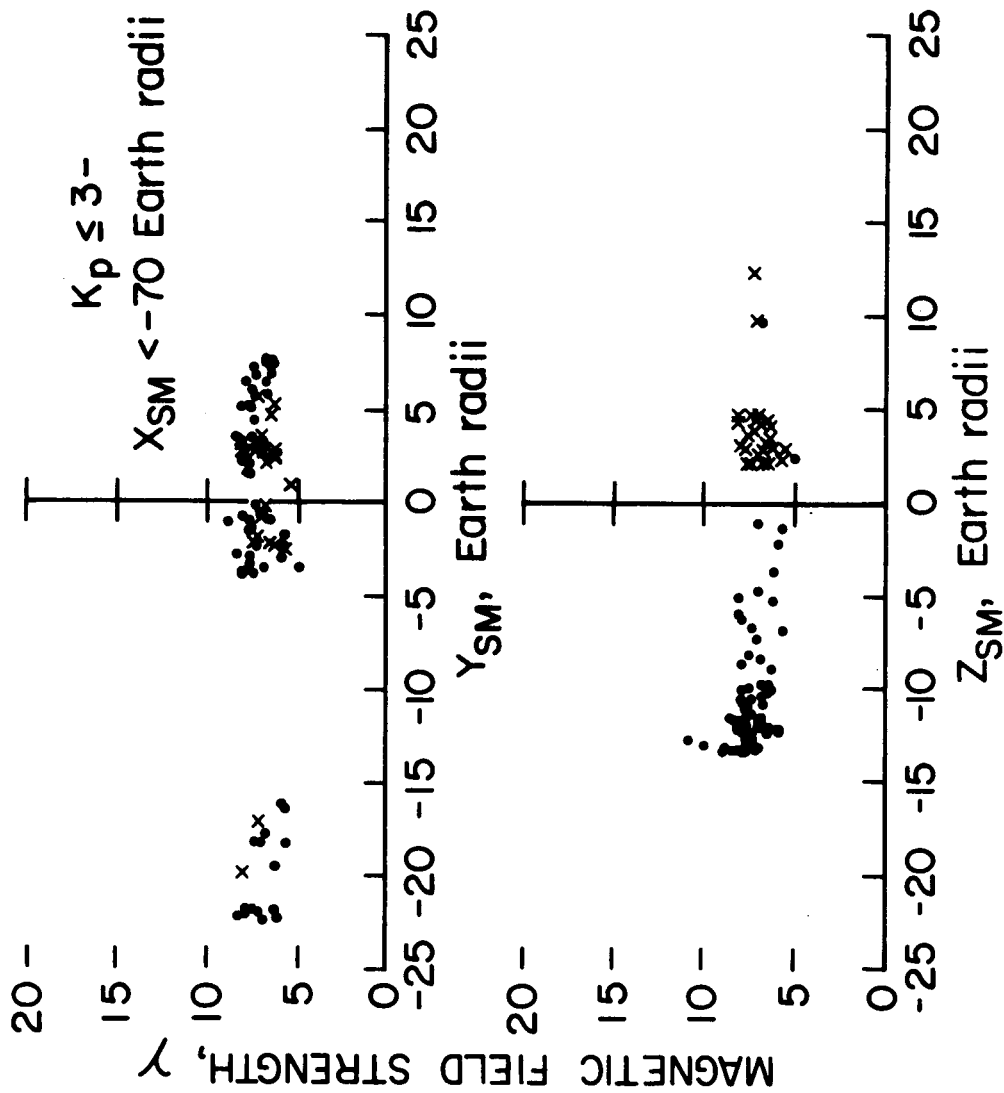


Fig. 17